Signal, Image and Video Processing
https://doi.org/10.1007/s11760-022-02287-z

ORIGINAL PAPER

Anti-light-leakage approach to CMOS sensor decorated on airborne platform

Hang Zhang[1] · Xin Chen[1] · Shuai Li[1] · Zhenya Sun[1] · Yue Li[1] · Yuquan Zheng[1] · Chao Lin[1]

Received: 25 September 2021 / Revised: 4 January 2022 / Accepted: 15 January 2022

Abstract
In order to avoid image degradation caused by rolling shutter distortion, CMOS imager sensors (CISs) with global shutter (GS) function are required to capture a picture of the fast moving scene. However, due to parasitic signal generated at the storage node of the GS CIS, the output of the sensor is degraded, which causes the sensor output varying hugely at the same exposure time but different frame rate. Then, the exclusive relationship between radiation intensity and sensor output cannot be obtained through radiometric calibration. The traditional approach is adding the light-shield structure for the storage node. We present here a new variable operation mode of the GS CIS, which makes it possible to automatically adjust the sequence of the sensor operating state on the basis of the relationship between exposure time and frame rate. This operation mode can ensure that the integrity of the stored signal is not compromised during the memory period. The accuracy of detection can be well improved. Furthermore, this new approach is proved valid by comparing the radiometric calibration results of traditional and new operation modes.

Keywords CMOS imager sensor · Global shutter · Light leakage · Exposure time · Frame rate

1 Introduction

CMOS image sensors (CISs) are nowadays widely used thanks to their advantages, such as low power consumption, low cost, improved noise and integrated readout circuit. The CIS is usually sorted by the different architectures, including rolling shutter (RS) pixel architecture and the global shutter (GS) pixel architecture [1, 2]. Because the GS CIS has the memory structure, additional MOS transistors and additional drive lines, GS CISs are generally inferior to RS ones in performance. However, imaging of a fast moving target cannot be done with the RS architecture. Especially for the airborne imaging spectrometer, the RS mechanism leads to severe motion distortion. Therefore, the GS pixel architecture is required; typically each GS pixel has an in-pixel charge storage node. After the integration time, the signal charge is transferred to this node. The storage node is generally built as a diffused diode, thus being susceptible to parasitic charge accumulation due to direct illumination by photons [3, 4]. In most case, there is a direct correlation between the parasitic charge number and the time signal charge stored on the storage node [5]. Light-shield structure for storage node is the most common approach currently. In this paper, a new variable operation mode is presented to prevent from light leakage of storage node. In Sect. 2, the mechanism of how light leakage generation occurs is summarized. In Sect. 3, the influence of light leakage on CISs for different frame rates is shown. In Sect. 4, the new operation mode is described in detail and the effects of different modes are compared.

Up to now, a variety of approaches have been developed to prevent the parasitic response on the storage node. For instance, a light-shield structure was placed upon the memory and an optimized shape light guide structure was placed upon the photodiode area, as it was reported by Kobayashi et al. [6, 7]. Tungsten buried light-shield (WBLS) process flow was introduced in CMOS storage gate, for wrapping around the storage gate (SG) to shield the storage node from incident light, as it was reported by Velichko et al. [3, 8]. Some similar approaches were introduced from the related patents by Gu [9]. These existing studies commonly focused on improvement of the sensor structure. However, the voltage

✉ Hang Zhang
zhanghang_ciomp@sina.com

✉ Chao Lin
linchaoluck@163.com

[1] Changchun Institute of Optics, Fine Mechanics and Physics, Chinese Academy of Sciences, Changchun 130033, China

Published online: 25 July 2022

of the storage node is a dynamic signal during normal operation; a tiny gap between the shield and storage area, caused by the untight connection between the light-shield board and storage node, will make it hard to eliminate the impact of parasitic charge on storage node wholly. Moreover, not all the sensors have the similar light blocking structure and the internal structures of the sensors from different manufacturers are often not in the control of the designer. In this paper, we solve the problem of parasitic charge accumulation on the storage node with sensor operation mode (time dimension), instead of sensor structure (spatial dimension).

2 Mechanism of the light leakage in CMOS sensor

The unit pixel of the CIS is the core device for imaging. The photodiode, the transfer gate, reset gate, the storage node and the light-shield structure are the standard components of a pixel. Photo-generated charge is acquired in the photodiode as the photosensitive element. At the end of the exposure period, the in-pixel storage is reset and the signal charge in the photodiode is transferred to the storage node. Owing to the increased MOS transistor count and additional storage node, the optical responsivity of GS pixel is reduced by the limited fill factor [10]. The integrity of the stored signal is an important contributing factor to limit the sensor's performance.

As shown in Fig. 1, the storage node in the pixel is the junction capacitance which is formed in the substrate between the transfer gate and the reset gate [9, 11]. Similar to the signal charge collected by photodiode, the parasitic charge is accumulated in the memory. Particularly, the storage node still accumulate parasitic charge after integration period. The signal charge that stays in the memory for a longer time will lead to more parasitic charge number created. In order to protect the stored signal from degradation, a light-shield structure is usually placed upon the storage area [12, 13].

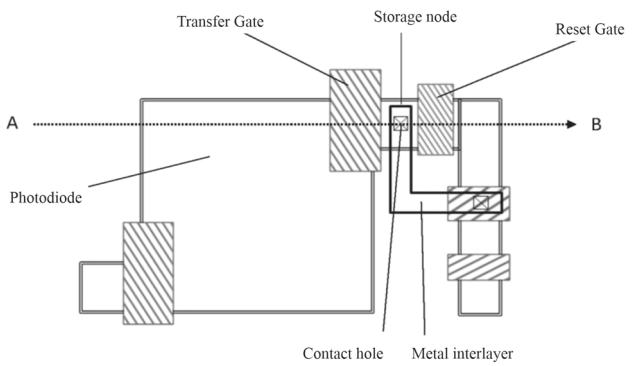

Fig. 1 The schematic diagram of a global pixel structure

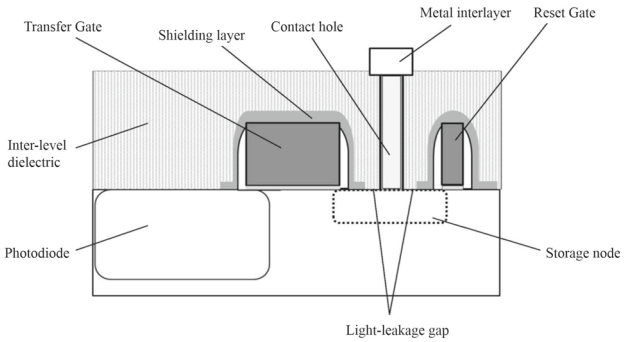

Fig. 2 The cross-sectional view of Fig. 1 along the A–B direction for global pixels structure

Further, Fig. 2 is the cross-sectional view of Fig. 1 along the A–B direction for global pixels structure [9]. There is a light-shield structure among the inter-level dielectric, usually fabricated by the metal materials such as tungsten, aluminum and copper, metals, as well as some metallic compound such as tantalum nitride. The light shield covers transfer gate, reset gate and storage node over large areas. However, the voltage of the memory is a dynamic signal during normal operation. Therefore, the contact hole of the storage node is not able to contact with the metal light shielding completely. A light-leakage gap is generated upon the storage node where there is no light shield or contact hole covered. The incident light could penetrate through the gap and generate parasitic charge on the storage node, leading to signal distortion and image quality decline [14].

3 Application of CMOS sensor on airborne spectrometer

For most imaging systems, the exposure time is approximately equal to frame period in order to maximize the radiance incident onto the sensor. When the scene is bright enough and the sensor output is saturated, exposure time would be shortened by increasing the frame rate. There is a close linkage relationship between exposure time and frame rate [15].

For the airborne imaging spectrometer, the frame rate of the sensor is determined by the flight speed of the airplane when the spatial resolution along the direction of flight is fixed. For example, the spatial resolution along the direction of flight is 1 m, the flight speed of the airplane is 100 m/s, and the frame rate is fixed to be 100 fps. The flight speed is usually fixed, and it does not change timely with the brightness variations, while exposure time needs to be adjusted at any time when the frame rate is fixed. In summary, the fixed flight speed and spatial resolution determine the frame rate, while the charging scenery causes different exposure time. According to the conventional operation mode, the signal

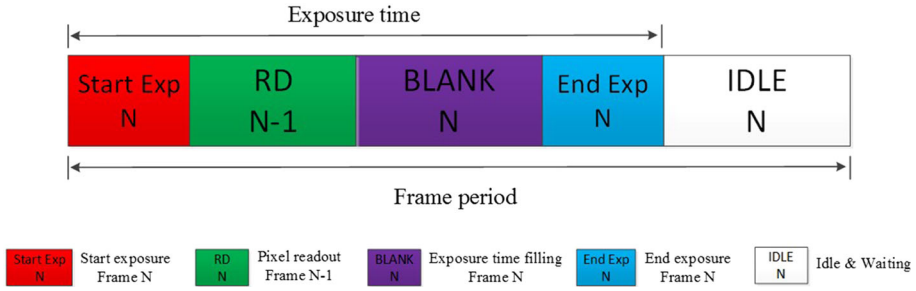

Fig. 3 The conventional operation mode of the global shutter CMOS sensor

charge is transferred to the storage node after charge collection and wait to readout until current frame ends. Based on the preceding section, the longer time signal charge waits in the memory, the more parasitic charge accumulates. This problem will lead to sensor output distortion and decline the calibration precision. Further, the corresponding relationship cannot be acquired accurately between radiation intensity and sensor output. In other words, for different frame rates, even in the same exposure time, the sensor output varies widely [16, 17].

In general, CMOS sensor has two operation modes: Integration Then Read (ITR) and Integration While Read (IWR). For the airborne imaging spectrometer, high frame rate is required, usually hundreds of frames per second, and the readout time is about several milliseconds. If ITR mode is selected, adjustable range of exposure time would be too small to adapt to scene brightness variations [18]. So here we just discuss how the operation mode of IWR influences the spurious response of the CMOS sensor.

For IWR mode, the conventional operation mode of the GS CMOS sensor is shown in Fig. 3.

SE(N) is the starting of exposure time for frame N; and EE(N) is the ending of the exposure time. The exposure time is the period from SE to EE, and the signal charge is transferred to storage node after EE. RD($N-1$) is the readout procedure of frame $N-1$; BLANK is used to supplement exposure time to make it achieve the setting value. Similarly, IDLE is used to supplement the frame period to make it match the flight speed.

The backside illuminated CIS GSENSE2020BSI from the Gpixel Inc. is selected as a sample to test. Table 1 lists the key specifications of this CIS.

Under the conventional operation mode, the radiometric calibration of this CIS is performed to obtain the relationship between the sensor output and the exposure time at different frame rates [19, 20].

The radiometric calibration scheme is shown in Fig. 4, consisting of an integrating sphere, a transfer radiometer, a CMOS camera and a quick-look system. The radiance of the integrating sphere is 0.1896 W/m^2/sr/nm to ensure the sensor works in the linear region with different exposure time. As radiometric standard, the radiometer FieldSpec 4 from

Table 1 Summarized specifications of GSENSE2020BSI

Parameter	Value
Pixel size	6.5 μm × 6.5 μm
Pixel array	2048 × 2048
Shutter type	Global shutter
Max frame rate	43 fps
Data rate	4.8 Gbps
Full well capacity	54 ke-
Dynamic range	90 dB
Quantization bits	12 bit

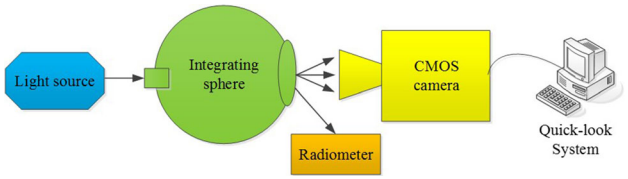

Fig. 4 The radiometric calibration scheme

Analytical Spectral Devices (ASD) Inc. is selected to monitor the output of the integral sphere. The quick-look system is used to store the image data of the camera. With the frame rates of 0.5 fps, 1 fps and 2 fps separately, 12 exposure times are adopted in the range of 0–20 ms, 100 frames of image data for each exposure time are averaged to reduce random error. As shown in Fig. 5, we can find the lower the frame rate (the longer the frame period) is corresponding to the larger the sensor output for the same exposure time.

This is because, for the same exposure time, longer frame period corresponds to longer the state of IDLE lasts. In other words, after the signal charge is transferred to storage node, more time is needed to wait to readout for longer frame period. Further, the sensor output difference between the frame rate of 0.5 fps and 1 fps is twice as big as that between the 1 and 2 fps. That is because the time difference of IDLE state has the same proportion approximately. In addition, the output difference between various frame rates decreases as the exposure time increases. The reason is that the proportion of the exposure time in the frame period increases

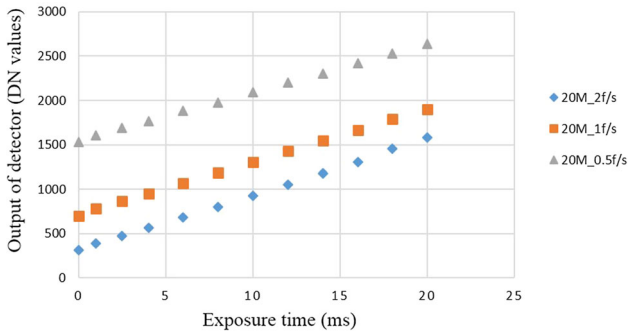

Fig. 5 The relationship between the sensor output and the exposure time for different frame rates with the conventional operation mode. In order to show the light leakage phenomenon obviously, the frame rate is reduced to increase the frame period

and the proportion of IDLE state decreases accordingly. So the light leakage phenomenon becomes weaker. The above results reflect the significant effect of parasitic charge collection during the memory period on the sensor output.

In order to reduce the spurious response of the storage node to light, a light-shield structure is usually placed to cover the memory. However, this method is unable to completely solve the light leakage as mentioned in Sect. 2.

4 New variable operation mode

In order to suppress spurious response when the signal charge is stored in memory, one variable operation mode of the GS CIS is proposed in this paper. Firstly, the frame rate is determined in accordance with flight speed. Then, the exposure time can be adjusted as the scene brightness changes, and the exposure time is divided into two ranges: $0-(T-T_{\mathrm{RD}})$ and $(T-T_{\mathrm{RD}})-T$, where T is frame period and TRD is readout time of one frame data.

Range1: $0-(T-T_{\mathrm{RD}})$

The CIS works according to the following state order: "SE(N)–BLANK(N)–EE(N)–RD(N)–IDLE(N)…" as shown in Fig. 6a. The state of BLANK(N) is used to fill the exposure time. The signal charge is readout immediately after charge integration.

Range2: $(T-T_{\mathrm{RD}})-T$

The CIS works according to the following state order: "SE(N)–RD2($N-1$)–BLANK(N)–EE(N)–RD1(N)–SE($N+1$)–RD2(N)–BLANK($N+1$)–EE($N+1$)……" as shown in Fig. 6b. The readout time of one frame image is divided into two parts: RD1 and RD2, which are placed on the current and next frame period, respectively. Their proportions in the entire readout time can be adjusted flexibly based on the different relationship between the exposure time and the frame period.

The following example is given to illustrate and verify the new operation mode:

The frame rate is set to 50fps, the readout time of one frame image is 3 ms, and the detailed operation mode is implemented by the following sequence of steps:

- The frame period is 1/50 fps = 20 ms; the exposure time is divided into two ranges: 0–17 ms and 17–20 ms.
- If the exposure time is set to 8 ms (in the first range), the Blank state between SE and EE is 8 ms, the readout time

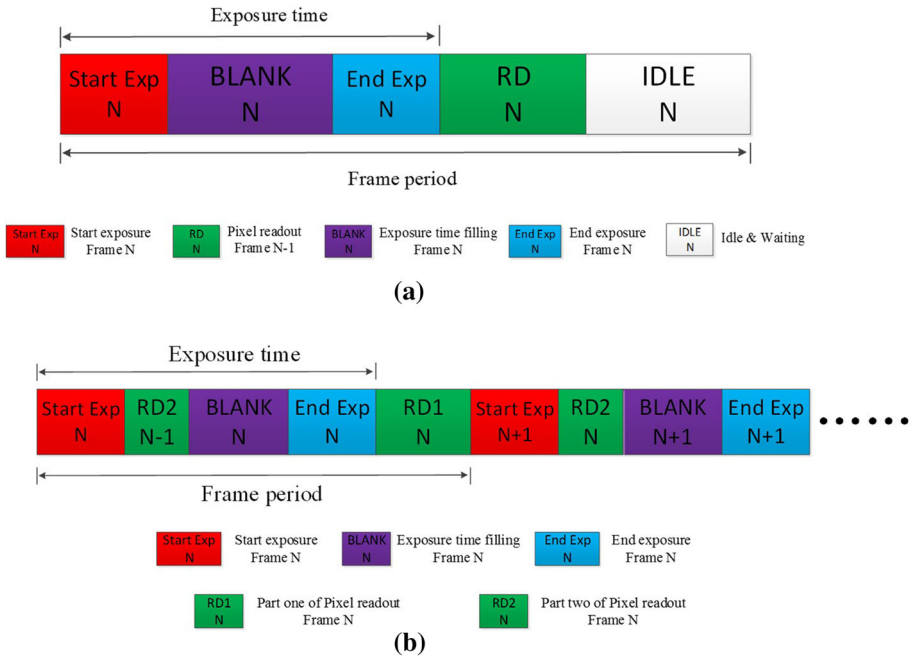

Fig. 6 The variable operation mode of the GS CIS. **a** The operation mode of the GS CIS for the exposure time with range of $0-(T-T_{\mathrm{RD}})$; **b** the operation mode of the GS CIS for the exposure time with range of $(T-T_{\mathrm{RD}})-T$

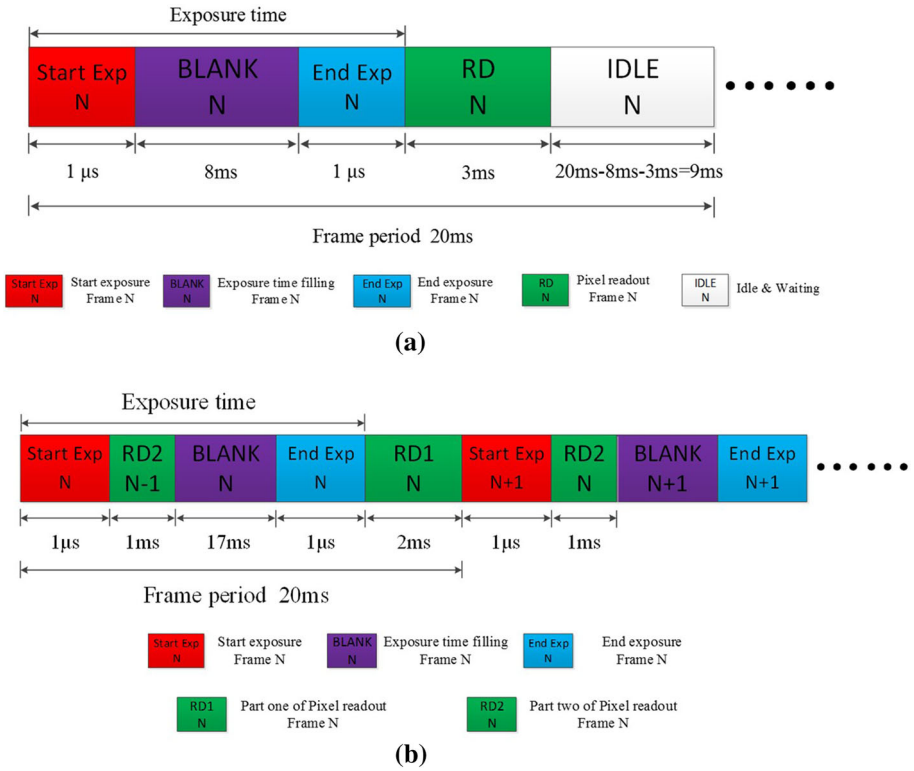

Fig. 7 One example to illustrate the new operation mode of the global CMOS sensor

of one frame image is fixed to 3 ms, and the IDLE state of 9 ms is used to fill the frame period, as shown in Fig. 7a.

- If the exposure time is set to 18 ms (in the second range), the time of RD1 is equal to frame period minus exposure time (20 ms − 18 ms = 2 ms), so the time of RD2 is 1 ms. The remaining exposure time is filled by the Blank state (17 ms), as shown in Fig. 7b.

The general idea of the new operation mode is that one frame data are readout immediately after charge integration and does not wait on the storage node at all. This approach can prevent the signal output of the GS CIS from being contaminated by parasitic charge collection in the memory.

Based on the new operation mode, the radiometric calibration of the camera is performed once more. As shown in Fig. 8, the outputs of the sensor are almost identical for different frame rates. It should be noted that the sensor output reduces obviously without parasitic charge. Hence, the radiance of the integrating sphere is increased to 0.4929 W/m^2/sr/nm for covering the entire sensor output range. Moreover, the sensor output is close to 0 when the exposure time is 0. By comparison, the DN value of the output is 337, 695 and 1524 for different frame rates with the conventional operation mode when the exposure time is 0.

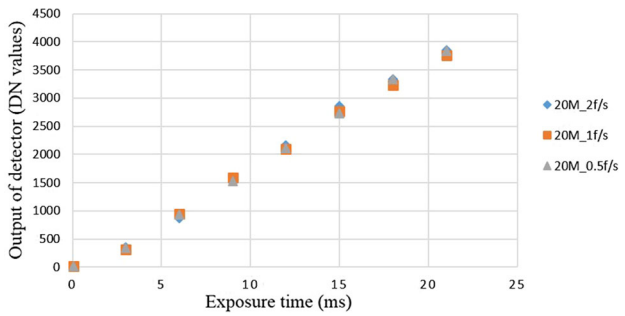

Fig. 8 The relationship between the sensor output and the exposure time at different frame rates by using the new variable operation mode

Compared with the conventional operation mode, the readout time of one frame image is divided into two parts for the new operation mode. The instruction of starting integration for the next frame is inserted between the two parts. Theoretically, the signal charge of the second part waits more time in the memory, resulting in nonuniformity of one frame image. However, there is no similar phenomenon observed in the experiment. This is because the instruction of starting integration is too short to effect the sensor output (less than 1 μs). The above experimental result verifies the feasibility of this new operation mode.

5 Conclusion

In this paper, a new approach is presented to avoid parasitic light for the memory in the GS pixel. The GS pixel structure and the traditional solution (with a light shielding) are illustrated. Combined with the characteristic of the airborne imaging spectrometer, the conventional operation mode of the GS CIS is described and the radiometric calibration is performed with different frame rates. The repercussions of the light leakage on the sensor output are reflected intuitively. In order to prevent the GS pixel from being susceptible to parasitic charge accumulation on storage node, a new operational mode of the sensor is introduced. The results of radiometric calibration with traditional and new operation modes are compared to verify the feasibility of the new approach.

Acknowledgements This research was funded by the Natural Science Foundation of Jilin Province, China, grant number 20200201203JC and the National Key Research and Development Program of China, Grant Number 2016YFB0500300.

References

1. Shoji, K., Min-Woon, S.: Noise reduction effect of multiple-sampling-based signal-readout circuits for ultra-low noise CMOS image sensors. Sensors **16**, 1867 (2016)
2. Claudio, B., Harald, H., Ivan, M.A., Samuel, B., Edoardo, C.: Single-photon avalanche diode imagers in biophotonics: review and outlook. Light Sci. Appl. **8**, 87 (2019)
3. Velichko, S., Hynecek, J., Johnson, R., Lenchenkov, V., Komori, H., Lee, H., Chen, F.: CMOS global shutter charge storage pixels with improved performance. IEEE Trans. Electron Devices **63**(1), 106–112 (2016)
4. David, K., Adam, M.H., Richard, C.P., Eric, O.P., Dmitry, A.F.: Infrared chemical imaging through non-degenerate two-photon absorption in silicon-based cameras. Light Sci. Appl. **9**, 125 (2020)
5. Wu, Z., Wang, X.: Stray light correction for medium wave infrared focal plane array-based compressive imaging. Opt. Express **28**(13), 19097–19112 (2020)
6. Sekine, H., Kobayashi, M., Onuki, Y., Kawabata, K., Tsuboi, T., Matsuno, Y.: Development of gentle slope light guide structure in a 3.4μm Pixel Pitch global shutter CMOS image sensor with multiple accumulation shutter technology. Sensors **17**, 2860 (2017)
7. Kobayashi, M., Onuki, Y., Kawabata, K., Sekine, H., Tsuboi, T.: A 1.8e−rms temporal noise over 110-dB dynamic range 3.4μm pixel pitch global-shutter CMOS image sensor with dual-gain amplifiers SS-ADC, light guide structure, and multiple-accumulation shutter. IEEE J. Solid-State Circuits **53**(1), 219–228 (2018)
8. Velichko, S., Agranov, G., Hynecek, J., Johonson, S., Komori, H.: Low noise high efficiency 3.75μm and 2.8μm global shutter CMOS pixel arrays. Proc. Int. Image Sensor Workshop 1–4 (2013)
9. Gu, X.: Global pixel structure for anti-light-leakage complementary metal oxide semiconductor (CMOS) image sensor, has contact hole whose upper ends are connected to first layer of metal interconnect layer to form composite light blocking structure. CN 109494232A (2019) (patent)
10. Yang, C., Ju, G., Chen, Y.: Study on the photo response of a CMOS sensor integrated with PIN photodiodes. Chin. Opt. **12**(5), 1076–1089 (2019)
11. Jiang, W., Zheng, T., Wu, B., Jiao, H., Wang, X., Chen, Y.: High-speed infrared imaging by an uncooled optomechanical focal plane array. Appl. Opt. **54**(34), 10189–10195 (2015)
12. Alexandre, L.R., Vincent, G., Olivier, M., Philippe, P., Federico, P.: Leakage current non-uniformity and random telegraph signals in CMOS image sensor floating diffusions used for in-pixel charge storage. Sensors **19**, 5550 (2019)
13. Guo, J., Li, J., Liu, C., Yin, Y., Wang, W., Ni, Z., Fu, Z., Yu, H.: High-performance silicon−graphene hybrid plasmonic waveguide photodetectors beyond 1.55μm. Light Sci. Appl. **9**, 29 (2020)
14. Alexandre, L.R., Cedric, V., Philippe, P., Jean-Marc, B., Serena, R.: Radiation-induced leakage current and electric field enhancement in cmos image sensor sense node floating diffusions. IEEE Trans. Nucl. Sci. **66**(3), 616–624 (2019)
15. Rubaiya, H., Mehmet, A.N., Getinet, W., Rodrigo, R.R.M., Pedro, A.M., Faiz, M.M.: An ultra-compact particle size analyser using a CMOS image sensor and machine learning. Light Sci. Appl. **9**, 21 (2020)
16. Wany, M., Paul, G.: CMOS image sensor with NMOS-only global shutter and enhanced responsivity. IEEE Trans. Electron Devices **50**(1), 57–62 (2003)
17. Lu, Q., Xu, Y., Wu, C., Qi, C.: Simulation analysis of error sensitivity factors in radiometric calibration of infrared hyperspectral interferometer. Opt. Precis. Eng. **28**(4), 867–877 (2020)
18. Woracek, R., Krzyzagerski, M., Markotter, H., Kadletz, P.: Spatially resolved time-of-flight neutron imaging using a scintillator CMOS-camera detector with kHz time resolution. Opt. Express **27**(18), 26218–26228 (2019)
19. Yi, X., Fang, W., Lin, Y., Wang, Y., Xu, N.: Experimental characteristics and measurement accuracy evaluation of space cryogenic absolute radiometric primary benchmark. Opt. Express **29**(1), 10–20 (2021)
20. Cui, C., Li, L., Li, Y., Guo, Y., Li, Y.: External calibration methods for geosynchronous ultraviolet-visible hyperspectral instrument. Opt. Express **29**(3), 484–492 (2021)